Supplementary information to:

High-temperature CO_2 capture by Li_4SiO_4: IR spectroscopic evidence for the double shell model.

Hoda Al Assaad,[a*]Khedidja Messabih,[b]Nadia Bendjaballah-Lalaoui,[b]Youcef Boucheffa,[c]Frédéric Thibault-Starzyk[a] and Arnaud Travert[a*]

a. Université de Caen Normandie, ENSICAEN, CNRS, Laboratoire Catalyse et Spectrochimie, 14000 Caen France

b. Laboratory of Material Chemistry, Catalysis and Environment, Faculty of Chemistry, University of Sciences and Technology Houari Boumediene (USTHB), BP 32, El-Alia, Bab-Ezzouar, Algiers, Algeria

ESI, S1. Chemical composition of Algerian natural diatomite before and after calcination

The Algerian natural diatomite (ND) used as the silica precursor in this study corresponds to the same material previously characterized in detail by Messabih et al.[1]. According to their analysis by X-ray fluorescence (XRF) spectroscopy (Rigaku ZSX Primus II X-ray spectrometer), this ND is mainly composed of silica (62.17 wt%), together with a significant amount of carbonates (~21.5 wt%) and several minor oxides (CaO, Al_2O_3, MgO, Fe_2O_3, Na_2O, and K_2O). Upon calcination at 800 °C for 3 h in air, the decomposition of carbonates leads to a partial enrichment in silica, increasing its content to 69.17 wt% while slightly concentrating the minor oxides. The detailed chemical composition of the raw and calcined ND samples is reported in Table S1.

Table S1 *: Chemical composition (wt %) of the Algerian natural diatomite (ND) before and after calcination at 800 °C for 3 h in air, determined by X-ray fluorescence (XRF). Data refer to the same ND sample characterized by Messabih et al. [1] and employed in this work as the silica precursor for Li_4SiO_4 synthesis.*

Materials	**Chemical composition (wt%)**										
	CO_3^{2-}	**Na_2O**	**MgO**	**Al_2O_3**	**SiO_2**	**P_2O_5**	**SO_3**	**K_2O**	**CaO**	**Ti_2O**	**V_2O_5**
ND	21.50	0.369	0.942	3.472	62.17	0.123	0.063	0.704	8.642	0.168	0.008
Calcined ND	12.249	0.427	1.077	3.822	69.171	0.132	0.064	0.836	9.995	0.203	0.010
Materials	**Chemical composition (wt%)**										
	Cr_2O_3	**MnO**	**Fe_2O_3**	**Co_2O_3**	**NiO**	**CuO**	**ZnO**	**RbO_2**	**SrO**	**ZrO_2**	
ND	0.022	0.008	1.491	0.003	0.006	0.002	0.003	0.003	0.022	0.008	
Calcined ND	0.033	0.009	1.835	0.002	0.009	0.001	0.006	0.004	0.026	0.008	

[1] K. Messabih, N. Bendjaballah-Lalaoui and Y. Boucheffa, *Environ Sci Pollut Res*, 2024, **31**, 32003–3201

Calcination effectively removes most carbonates, enhances the relative SiO_2 content, and slightly concentrates other oxides such as CaO, MgO, and Fe_2O_3, which later contribute to the formation of minor silicate phases ($Li_2Ca_2Si_2O_7$, Li_2MgSiO_4, and Li_3AlSiO_5) detected by XRD in the calcined Li_4SiO_4 samples.

ESI, S2. Textural and structural properties of the Li_4SiO_4 samples

The Li_4SiO_4 powders investigated in the present study were synthesized by the solid-state route described in the main text. The detailed structural and textural characterizations of these samples were previously reported by Messabih et al.[1] using the same materials and synthesis conditions. A concise summary of their main findings is provided below for completeness and to ensure that all information relevant to the present work is accessible within the same article.

S2.1. Structural characterization (XRD)

The Structural characterization of the Li_4SiO_4 powders used in the present study were previously investigated by Messabih et al. [1] using the same samples (SiO_2-LS, ND-LS, and 10% ND-LS) synthesized under identical experimental conditions. X-ray diffraction (XRD) patterns of the Li4SiO4 samples were obtained with a PANalytical-X'Pert PRO diffractometer using Cu-Kα radiation (λ = 1.54060 Å) over a 2θ range of 3–70°. The identification of crystalline phases was determined conventionally by High Score plus software basing on the Joint Committee Powder Diffraction Standards (JCPDS) database.

Powder X-ray diffraction (XRD) analyses confirmed the formation of monoclinic Li_4SiO_4 (JCPDS 29-0829) as the dominant crystalline phase in all samples (SiO_2-LS, ND-LS, and 10% ND-LS). Minor reflections corresponding to Li_2SiO_3 and Li_2CO_3 were detected in the SiO_2-LS reference, suggesting incomplete lithiation of SiO_2 at 700 °C. For samples synthesized with natural diatomite (ND-LS and 10% ND-LS), additional weak peaks were observed and attributed to secondary silicate phases such as $Li_2Ca_2Si_2O_7$, Li_2MgSiO_4, and Li_3AlSiO_5, originating from the minor oxides present in the ND precursor (see ESI, S1). The Semi-quantitative contents of the different predominant phases obtained from XRD patterns are summazired in Table S2.

***Table S2** : Semi-quantitative contents of the different predominant phases obtained from XRD patterns for SiO_2-LS, ND-LS and 10% ND-LS samples. Data adapted from Messabih et al.[1] for the same materials and synthesis conditions.*

	Content(wt%)						
Phases	**Li_4SiO_4**	**Li_2SiO_3**	**$Li_2Si_2O_5$**	**Li_2MgSiO_4**	**$Li_2Ca_2Si_2O_7$**	**Li_3AlSiO_5**	**SiO_2**
SiO_2-LS	62	18	7	--	--	--	13
ND-LS	41	11	8	13	16	11	--
10% ND-LS	48	10	8	12	18	4	--

S2.2. Textural characterization (BET analysis)

Nitrogen adsorption–desorption isotherms were recorded at −196 °C using a Micromeritics ASAP 2020 instrument. All samples displayed type II isotherms, typical of nonporous to macroporous aggregates. The specific surface area, pore volume, and average pore diameter values are summarized in Table S3.

***Table S3**: Textural properties of the Li_4SiO_4 samples synthesized with pure SiO_2 and natural diatomite (ND) precursors, as determined from N_2 adsorption–desorption isotherms at −196 °C. BET surface area, total pore volume, and mean pore diameter values are listed. Data adapted from Messabih et al.[1] for the same materials and synthesis conditions.*

Sample	BET surface area ($m^2.g^{-1}$)	Pore volume ($cm^3.g^{-1}$)	Mean pore diameter (nm)
SiO_2-LS	2.57	0.01	15.4
ND-LS	4.61	0.017	14.7
10% ND-LS	5.72	0.022	15.2

The incorporation of natural diatomite clearly enhances the surface area and pore volume compared to the pure SiO_2-based Li_4SiO_4. This improvement is attributed to the inherited porosity and better dispersion of ND particles during the solid-state reaction.

S2.3. Morphological characterization (SEM)

The morphological characteristics of the Li_4SiO_4 powders used in the present study were previously investigated by Messabih et al. [1] using the same samples (SiO_2-LS, ND-LS, and 10% ND-LS) synthesized under identical experimental conditions. Their SEM analysis provided valuable information on the particle size and morphology of these materials. Although the micrographs are not reproduced here, the particle size distribution was determined from the SEM images using ImageJ software, based on the measurement of 60 individual particles for the 10% ND-LS sample. The particles exhibited diameters ranging from 3.7 to 30 µm, with an average size of approximately 10 µm. All sorbents consisted mainly of agglomerates of granular and polyhedral grains, a morphology typical of Li_4SiO_4 powders obtained via solid-state synthesis. These microstructural characteristics are therefore directly representative of the materials employed in the present study.

ESI, S3. Complete FTIR spectra of pure Li_2CO_3 and SiO_2

Figure S1 and S2 presents the complete FTIR spectra of pure lithium carbonate (Li_2CO_3) and pure silicon dioxide (SiO_2) powders, respectively, recorded in transmission mode at room temperature. These reference spectra were used to identify and assign the vibration bands involved in the calibration of carbonate features described in the main text (Figure 1).

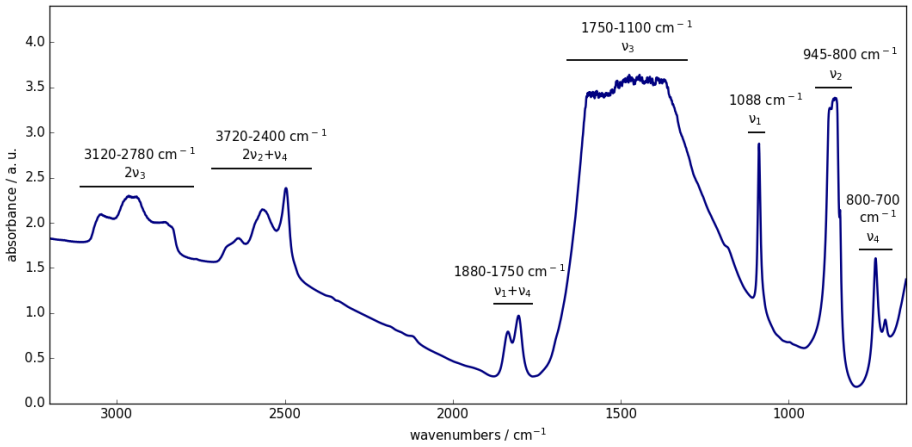

Figure S1 : FTIR spectrum of pure Li_2CO_3 pellet used for calibration.

The spectrum of Li_2CO_3 (Figure S1) exhibits the six characteristic vibration modes of the CO_3^{2-} ion. The overtones and combination bands are observed between 3150 and 2400 cm^{-1}, corresponding respectively to $2\nu_3$ and $2\nu_2 + \nu_4$ transitions. The $\nu_1 + \nu_4$ combination band appears in the 1880–1750 cm^{-1} region, while the intense asymmetric stretching ν_3 mode is found between 1750 and 1100 cm^{-1}. The ν_1 symmetric stretching band of Li_2CO_3 is centered at ~1088 cm^{-1}, and the bending modes ν_2 and ν_4 are located in the 945–800 cm^{-1} and 800–700 cm^{-1} regions, respectively.

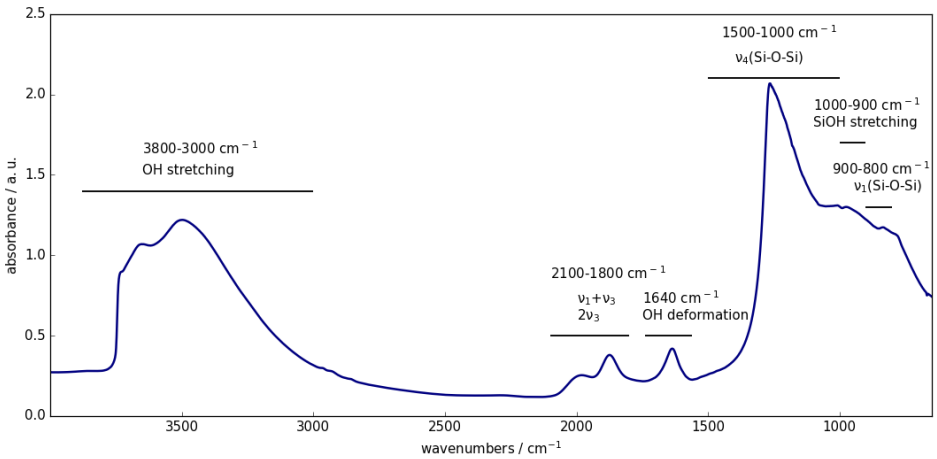

Figure S2 : FTIR spectrum of pure SiO_2 pellet used for calibration

The spectrum of SiO_2 (Figure S2) is dominated by the characteristic vibrations of the silicate network. The broad band between 3800 and 3000 cm^{-1} corresponds to the stretching vibration of hydroxyl groups (O–H) from surface silanols and adsorbed water. A weaker band centered near 1640 cm^{-1} is assigned to the $\delta(H_2O)$ bending mode of molecular water. The spectral region between 2100 and 1800 cm^{-1} contains weak combination bands ($\nu_1 + \nu_3$ and $2\nu_3$) of Si–O–Si stretching vibrations. The main absorption band between 1500 and 1000 cm^{-1} is attributed to the asymmetric stretching vibration ν_4(Si–O–Si), while the shoulder observed around 900–800 cm^{-1} corresponds to the symmetric stretching ν_1(Si–O–Si). The feature near 1000–900 cm^{-1} is assigned to terminal Si–OH stretching vibrations. All these bands are consistent with typical spectra of amorphous silica.

ESI, S4. General and detailed views of the "Jumpipe" IR cell

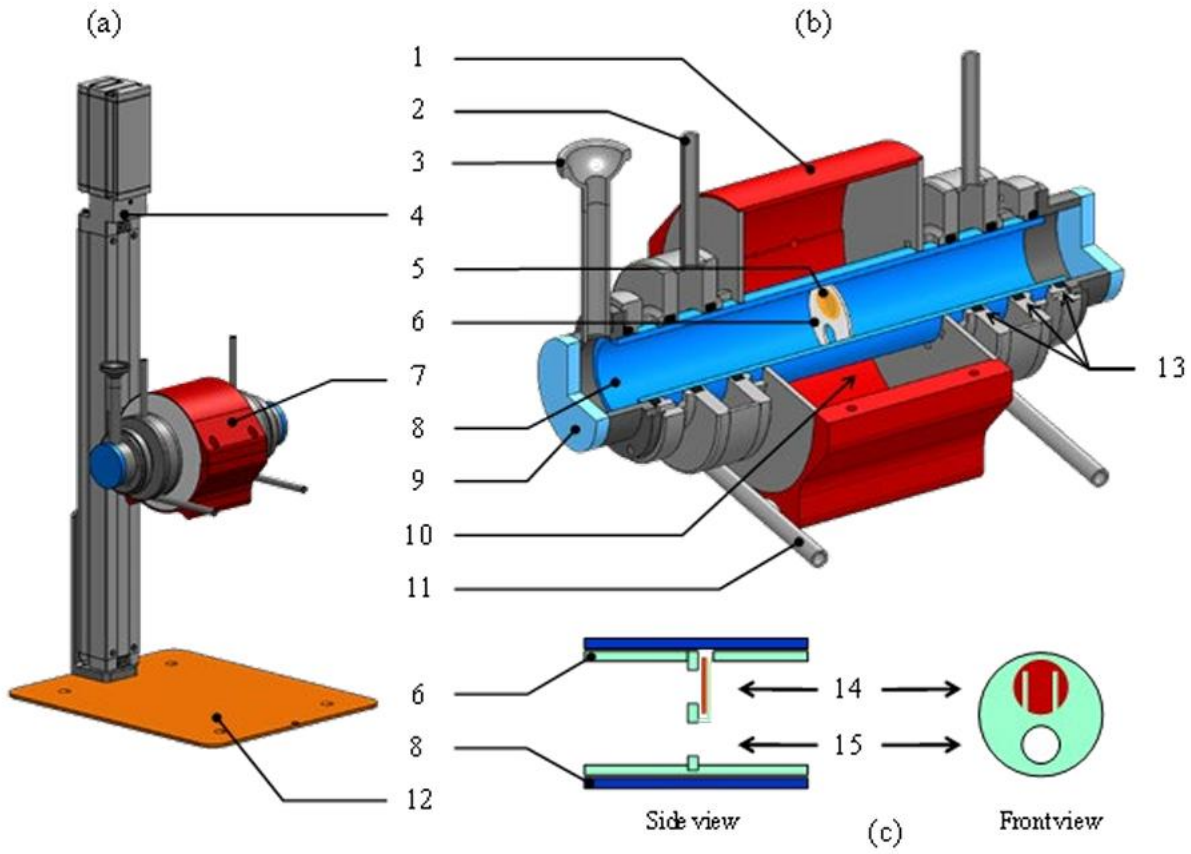

Figure S3 : General (a) and detailed (b) views of the "Jumpipe" IR cell. (c) Schematic diagram of the quartz sample holder [2].

1 – Outer casing
2 – Air cooling inlet
3 – Connection to the vacuum system
4 – Motorized translation stage
5 – Sample (13 mm diameter pellet)
6 – Two-position sample holder
7 – Removable IR cell for glovebox sample handling
8 – Quartz tube
9 – KBr window for the IR beam
10 – Furnace location
11 – Air cooling outlet
12 – Spectrometer base plate
13 – Kalrez O-ring
14 – IR beam path for sample spectrum acquisition
15 – IR beam path for gas-phase spectrum acquisition.

The main body of the cell consists of a quartz cylinder housing a two-position sample holder at its center: the “sample position,” where the IR beam passes through the catalyst pellet to record the spectrum of the sample, and the “gas position,” where the spectrometer records the gas-phase spectrum

ESI, S5. Powder X-ray diffraction (XRD) analysis

The diffraction pattern of SiO_2–LS after calcination (Figure S4, left) shows the characteristic reflections of the monoclinic Li_4SiO_4 phase, confirming the formation of a single, well-crystallized orthosilicate. No reflections associated with Li_2CO_3 are detected, in agreement with FTIR observations that carbonate residues remain limited to minor surface species. After CO_2 exposure, the corresponding pattern (Figure S4, top) clearly shows the emergence of reflections attributed to Li_2SiO_3 and Li_2CO_3, consistent with the overall carbonation pathway (equation 1).

For the ND-derived material (10 % ND–LS), the calcined sample (Figure S5, bottom) also exhibits Li_4SiO_4 as the dominant phase, accompanied by weak reflections corresponding to minor secondary silicates (Li_2MgSiO_4 and $Li_2Ca_2Si_2O_7$), already identified in the pristine diatomite precursor (ESI, S2). After CO_2 capture (Figure S4, top), additional reflections of Li_2SiO_3 and Li_2CO_3 appear, confirming the same global transformation as for SiO_2–LS. No distinct peaks associated with $MgCO_3$ can be resolved in the diffraction patterns, due to strong overlap between the principal reflections of $MgCO_3$ and Li_2SiO_3 in the $2\theta \approx 31–36°$ region.

These XRD results thus confirm that Li_4SiO_4 is the predominant crystalline phase after calcination, and that CO_2 capture leads to the $Li_4SiO_4 + CO_2 \rightarrow Li_2SiO_3 + Li_2CO_3$ transformation in both SiO_2- and ND-derived materials. The partial carbonation of Mg-bearing silicates, undetectable by XRD but evidenced by FTIR, provides additional insight into the local microstructural complexity of ND-based sorbents.

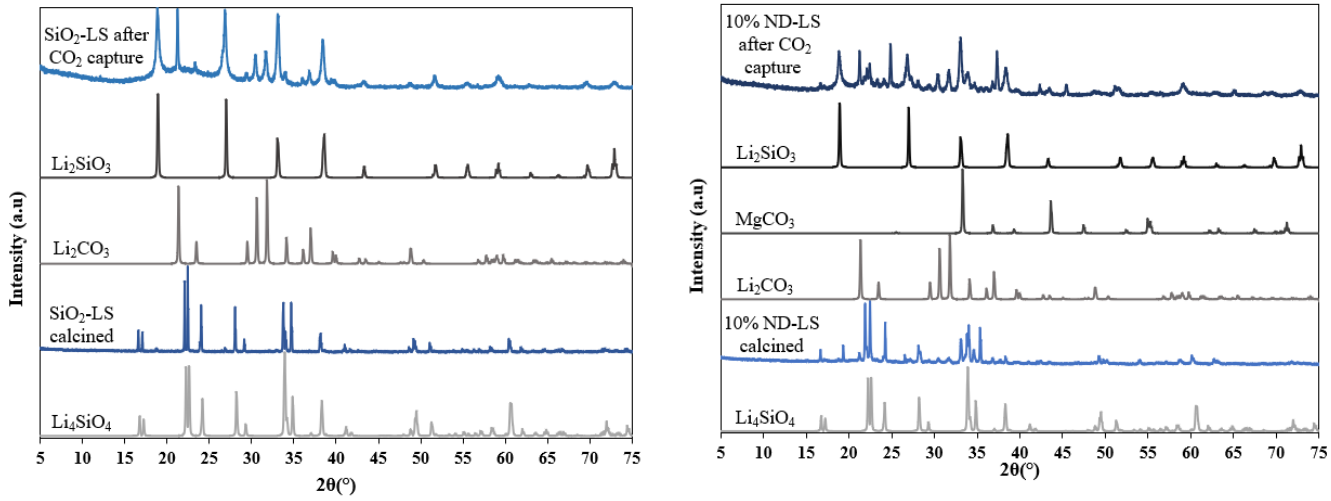

Figure S4 : Powder XRD patterns of SiO_2–LS (left) and 10 % ND–LS (right) before and after CO_2 capture at 500 °C. The calcined samples (bottom) show the characteristic reflections of Li_4SiO_4, while the post-capture patterns (top) exhibit additional reflections assigned to Li_2SiO_3 and Li_2CO_3. Reference diffraction patterns of Li_4SiO_4, Li_2SiO_3, Li_2CO_3, and $MgCO_3$ are shown for comparison.

ESI, S6. TG/DSC analysis

Prior to CO_2 capture, the samples were first heated to 600 °C under a nitrogen flow and maintained at this temperature to ensure complete decarbonation and thermal activation (see temperature program, Figure S5A). The CO_2 capture process was then studied by heating from 30 °C to 600 °C under a CO_2 atmosphere. TG analyses revealed a significantly earlier onset of CO_2 uptake in samples derived from natural diatomite (ND) compared to those prepared from pure silica (see TG curves, Figure S5C). This

early uptake in ND-based samples is accompanied by a distinct endothermic peak centered at approximately 475 °C in the DSC signal (Figure S5E), which is likely associated with the formation of a eutectic mixture specific to the ND-derived materials.

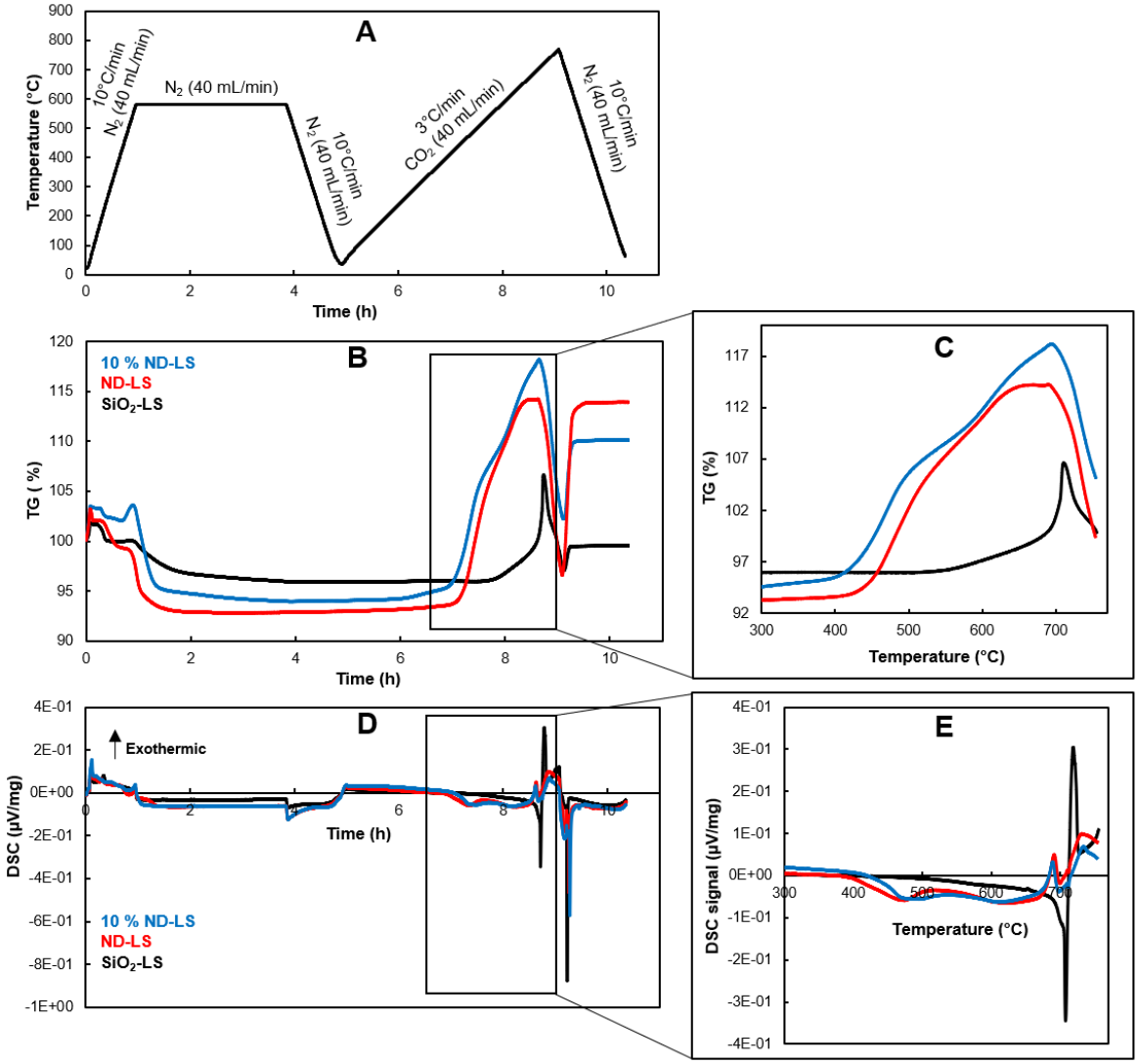

Figure S5 : (A) Thermal program used for TG/DSC measurements under N_2 and CO_2 atmospheres. (B) Thermogravimetric (TG) profiles of SiO_2–LS, ND–LS, and 10% ND–LS samples as a function of time. (C) Zoom view of the CO_2 capture stage showing the TG signal as a function of temperature. Because the mass axis was not re-normalized after each intermediate step (activation and cooling), the relative starting point of the capture curves appears below 100%. This is purely an artifact of data representation and does not affect the reliability of the measured mass variations, which remain consistent with the full TG traces. (D) Differential scanning calorimetry (DSC) signals recorded simultaneously during the TG experiments. (E) Zoom view of the DSC signal during the CO_2 capture stage.

ESI, S7.

The spectral contributions of species 1 and species 2 for each sample were determined using two complementary methods for validation purposes. The first method involved combining the pure component spectra with their respective concentration profiles obtained from the MCR-ALS analysis; the results are presented in Figure 7 of the main text. Since species 2 only forms once the concentration of

species 1 has stabilized, its spectral contribution can also be estimated by subtracting the final spectrum of species 1 from the experimental spectra recorded over time. For the ND-derived samples, this subtraction is valid up to 70 minutes, whereas for samples prepared from SiO_2, it remains valid up to 120 minutes. In this approach, the contribution of species 1 corresponds to the early spectra, and species 2 is obtained from the residual signal after subtraction of the final spectrum of species 1 (Figure S6). To compare the results from both methods, Figure S7 shows the carbonate percentage as a function of CO_2 pressure for SiO_2-LS, ND-LS, and 10% ND-LS samples, calculated from both the subtraction method and the MCR-ALS analysis. The close agreement between the two sets of results confirms the validity and consistency of both approaches.

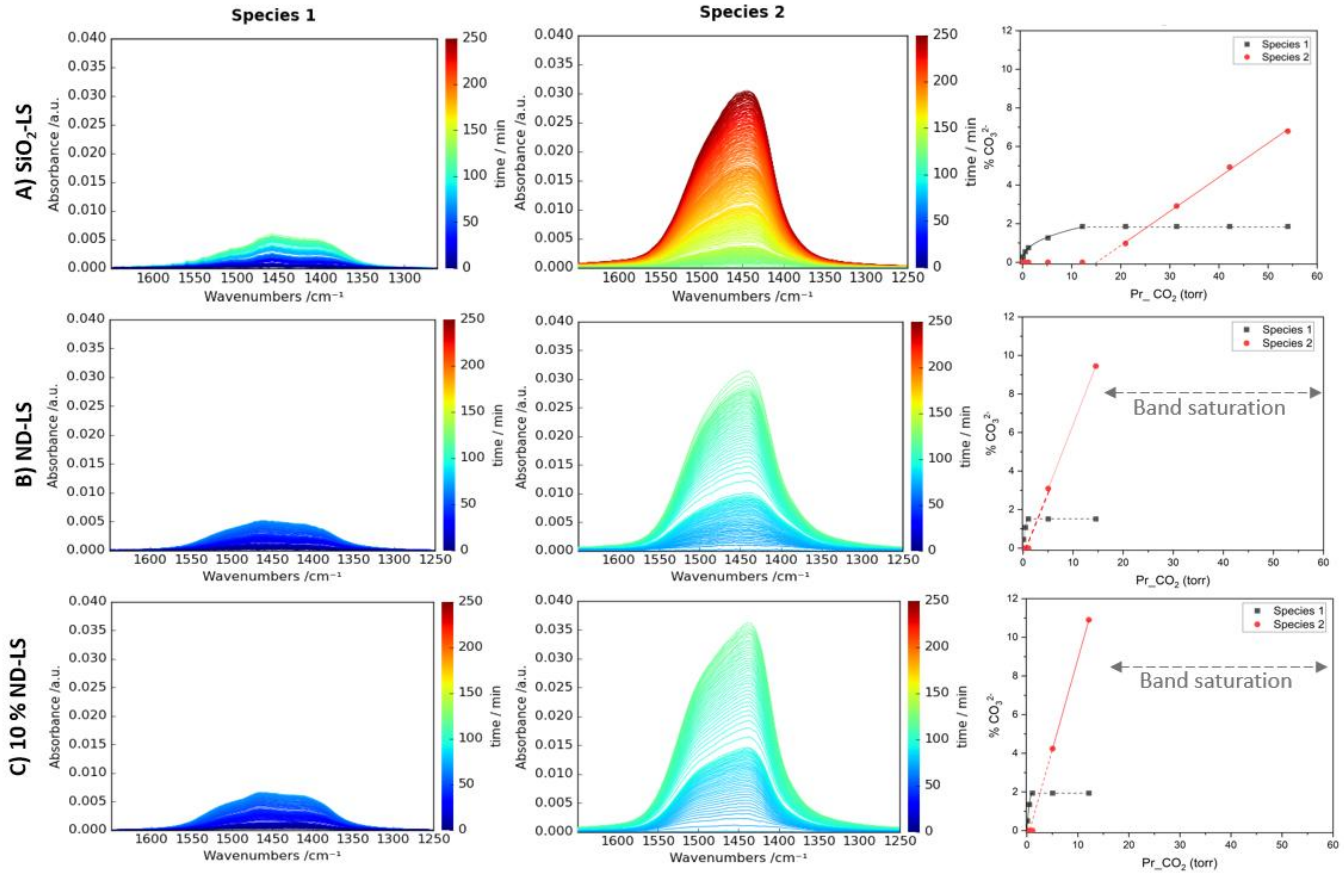

Figure S6 : Spectral contributions of species 1 and 2 along with the corresponding carbonate percentage as a function of CO_2 pressure for SiO_2-LS, ND-LS, and 10% ND-LS, respectively.

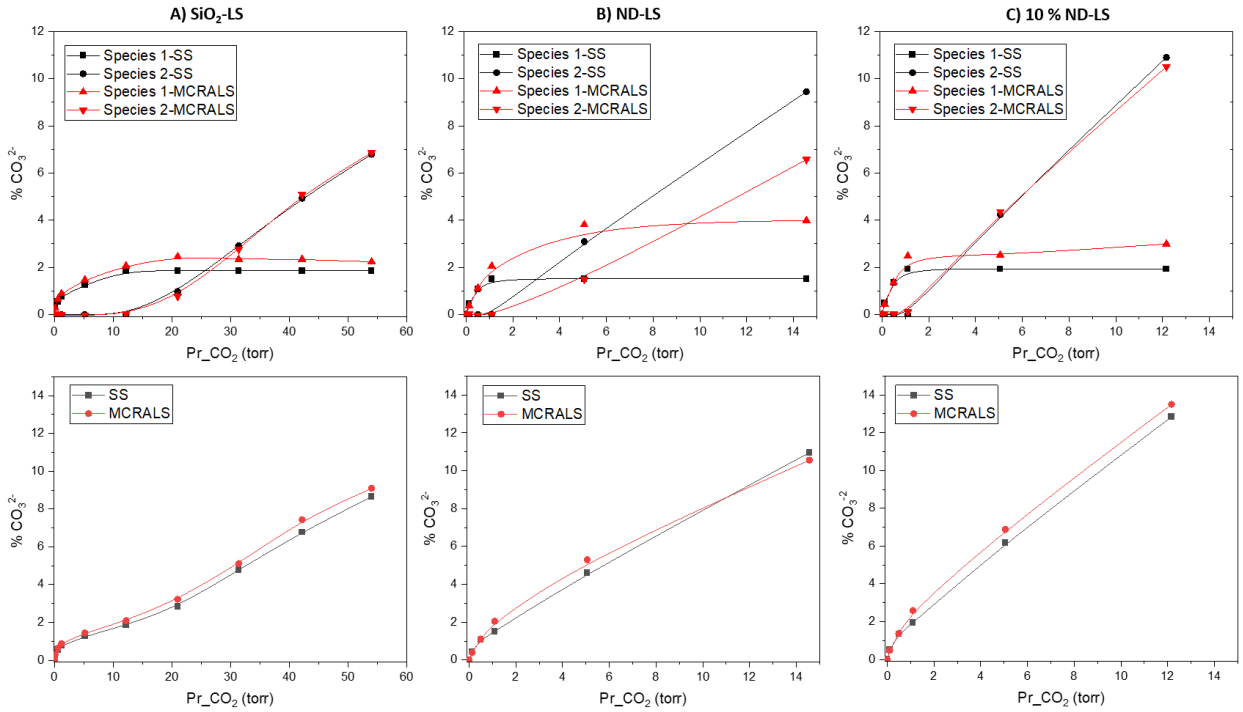

Figure S7 : Carbonate percentage for species 1, species 2 and the total carbonate content as a function of CO_2 pressure for SiO_2-LS, ND-LS and 10% ND-LS samples, calculated using both the subtraction method and the MCR-ALS analysis.